Modal Analysis of Chushandian Gravity Dam

Liu Jiabing [a*]

[a] *School of Water Conservancy, North China University of Water Resources and Electric Power, Zhengzhou-450045, China.*

Author's contribution

The sole author designed, analysed, interpreted and prepared the manuscript.

Original Research Article

ABSTRACT

This article uses the finite element software ABAQUS to establish a three-dimensional finite element model based on the overflow dam section 12 # ~15 # and surface outlet dam section of the Chushandian gravity dam. The stress and displacement distribution of the 12 # ~15 # dam section of the Chushandian gravity dam under normal water storage level are analyzed; On this basis, modal analysis is conducted on the 12 # ~15 # dam section to study the impact of the dam's own modal conditions on the normal operation of the dam. The research shows that: (1) Under the condition of normal height water level, there is a small tensile stress at the dam heel, and the compressive stress at the dam toe is within the normal range. There is significant stress at the intersection of the upper curved part of the overflow dam and the transverse joint. The dam body strength meets the requirements and can be considered safe for the reservoir. (2) Modal analysis of the model reveals that significant deformation can occur at the right side of the dam crest during lower frequency vibrations. With the increasing frequency, the easily deformed parts of the dam are still at the top of the dam, and the displacement of the easily deformed parts is increasing. The position of the easily deformed parts is moving along the Dam axis, and the deformation direction of the easily deformed parts will change regularly.

_____

Corresponding author: Email: 1441710848@qq.com;

1. INTRODUCTION

Gravity dams are usually large concrete structures, characterized by low tensile strength, high compressive strength, and susceptibility to cracking. In addition, gravity dams are generally not equipped with steel bars. Once tensile stress occurs in certain parts of the dam, it depends on the strength of the material to withstand it [1-4]. There are many examples of dam failures, such as the Khadkawasla Dam and Panshet Reservoir [5], which have resulted in downstream reservoir failures due to upstream reservoir failures. After the dam failure of the upstream reservoir, all the accumulated water in the upstream reservoir flows into the downstream reservoir, and the downstream reservoir is damaged by a huge force due to its lower flood discharge capacity than the upstream [6]. In 1997, due to the impact of heavy rainfall, Shanxi Province also experienced a situation where the upstream reservoir collapsed, causing the downstream Pingtou Reservoir to overflow and subsequently collapse. The dam accident [7] has had a huge impact on downstream people, resulting in a decrease in population, stagnant economic development, and an increase in unemployment, as shown in Figs. 1 and 2. Because the consequences of a dam failure are particularly serious, studying the stress distribution and stability of a gravity dam is of great significance for the normal operation and downstream of the dam.

Fig. 1. Banqiao reservoir crash

The stress analysis of gravity dams in current design specifications adopts the method of material mechanics [8-10]. The material mechanics method ignores the influence of foundation deformation and different materials in different parts of the dam body when considering the stress of the dam body. In addition, the material mechanics method adopts many assumptions, resulting in a significant difference between the calculated stress and the actual situation. Since the 1960s, the emergence of finite element method has made up for the shortcomings of material mechanics method, greatly reducing the phenomenon of inconsistency between calculation and actual situation. When the geological conditions of the dam are complex or the materials in different parts of the dam body are different, finite element methods can be used for boundary treatment and material zoning. The finite element method, combined with computer calculations, can visually observe the stress distribution of the entire dam section and provide reliable constructive suggestions for the construction of the dam. The combination of finite element method and computer use has made finite element simulation analysis the preferred method for studying gravity dams.

Fig. 2. St. Francis dam break

Based on this, this paper, based on ABAQUS software and finite element method, conducts finite element modeling analysis on the typical dam section of Chushandian gravity dam located in Xinyang City, and analyzes its stress, displacement distribution and dam vibration under the condition of normal height water level. Finally, it conducts anti sliding stability safety analysis on the 15 # dam section. Through finite element analysis, it is possible to understand the stress and stability of typical sections of the Shandian gravity dam, and to provide constructive suggestions for the structure of the dam.

2. FUNDAMENTAL THEORY

2.1 Basic Equations of Elasticity

During the construction of the pipeline, it is easy to collapse and collapse pits in the shallow part. Through the finite element method, elasticity

provides the principle and method of calculation for solving. Elasticity is closely related to finite element method. The answer to elasticity is a general answer to practical problems in elasticity. The finite element solution is a concrete answer to practical elastic mechanics problems [11]. When using finite element software to solve practical objects, the equations of elasticity are first used, and then the equations in actual situations are calculated and solved. The differential unit body is shown in Fig. 3, and the three basic equations of the elastic mechanics method are obtained as follows:
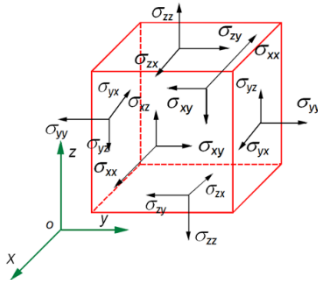

Fig. 3. Differential unit body

(1) Equilibrium differential equation

The equilibrium differential equation mainly considers the static equilibrium of various micro elements inside an object, establishing the relationship between internal stress and external physical force.

$$\frac{\partial \sigma_x}{\partial x} + \frac{\partial \tau_{yx}}{\partial y} + \frac{\partial \tau_{zx}}{\partial z} + X = 0$$
$$\frac{\partial \tau_{xy}}{\partial x} + \frac{\partial \sigma_y}{\partial y} + \frac{\partial \tau_{zy}}{\partial z} + Y = 0 \tag{1}$$
$$\frac{\partial \tau_{xz}}{\partial x} + \frac{\partial \tau_{yz}}{\partial y} + \frac{\partial \sigma_z}{\partial z} + Z = 0$$

(2) Geometric equation

The geometric equation mainly considers the relationship between the differential units inside the object.

$$\varepsilon_x = \frac{\partial u}{\partial x}, \gamma_{xy} = \frac{\partial v}{\partial x} + \frac{\partial u}{\partial y}$$
$$\varepsilon_y = \frac{\partial v}{\partial y}, \gamma_{yz} = \frac{\partial w}{\partial y} + \frac{\partial v}{\partial z} \tag{2}$$
$$\varepsilon_z = \frac{\partial w}{\partial z}, \gamma_{zx} = \frac{\partial w}{\partial x} + \frac{\partial u}{\partial z}$$

(3) Physical equation

The physical equation considers the condition of consistent stress and strain among the differential elements inside the object.

$$\varepsilon_x = \frac{1}{E}\left[\sigma_x - \mu\left(\sigma_y + \sigma_z\right)\right], \gamma_{xy} = \frac{\tau_{xy}}{G}$$
$$\varepsilon_y = \frac{1}{E}\left[\sigma_y - \mu\left(\sigma_x + \sigma_z\right)\right], \gamma_{yz} = \frac{\tau_{yz}}{G} \tag{3}$$
$$\varepsilon_z = \frac{1}{E}\left[\sigma_z - \mu\left(\sigma_x + \sigma_y\right)\right], \gamma_{zx} = \frac{\tau_{zx}}{G}$$

$$G = \frac{E}{2(1+\mu)} \tag{4}$$

2.2 Basic Principles of Finite Element Method

When using the finite element method to solve, the continuum should first be discretized into a finite number of differential elements, and then the basic equations of elasticity should be used to create the relationship between various physical quantities and node displacements within the differential elements. After synthesizing the overall stiffness, the virtual work principle is used to introduce boundary conditions for solution [12].

Basic quantities in finite element method:

$$\{d\} = \begin{bmatrix} u & v & w \end{bmatrix}^T \tag{5}$$

$$\{\sigma\} = \begin{bmatrix} \sigma_x & \sigma_y & \sigma_z & \tau_{xy} & \tau_{yz} & \tau_{zx} \end{bmatrix}^T \tag{6}$$

$$\{\varepsilon\} = \begin{bmatrix} \varepsilon_x & \varepsilon_y & \varepsilon_z & \gamma_{xy} & \gamma_{yz} & \gamma_{zx} \end{bmatrix}^T \tag{7}$$

Basic steps of finite element method:

(1) Discretization of structure: the object is transformed into a small unit in a decentralized state through the division of differential units. And it is believed that the medium for transmitting force between each differential element is a node by node.

(2) Unit analysis: The main content of unit analysis is to establish the relationship between the basic quantities of differential units. The relationship between various physical quantities is as follows:

① Unit displacement mode

$$\{d\} = [N]\{\delta\}^e \tag{8}$$

② Unit strain

$$\{\varepsilon\} = [B]\{\delta\}^e \tag{9}$$

③ Unit stress

$$\{\sigma\} = [D][B]\{\delta\}^e = [S]\{\delta\}^e \quad (10)$$

Where, $[B]$ represents the element geometric matrix, $[D]$ represents the element elastic matrix, and $[S]$ represents the element stress matrix.

④ According to the principle of virtual work, node forces can be expressed as:

$$\{F\}^e = [k]\{\delta\}^e \quad (11)$$

$$[k] = [B][D]^T[B]dxdydz \quad (12)$$

⑤ Equivalent node load

$$\{F_l\}^e = [N]^T\{Q\} + [N]^T\{\bar{P}\}dA + [N]^T\{P\}dV \quad (13)$$

where, $[N]$ represents the shape function, $\{Q\}$ represents the displacement of concentrated force towards the node, $\{\bar{P}\}$ represents the displacement of surface force towards the node, and $\{P\}$ represents the displacement of physical force towards the node.

(3) Overall analysis

The overall analysis is conducted on a finite element composed whole, mainly involving the introduction of edges, the synthesis of total stiffness, and the establishment of a system of overall equilibrium equations. The overall equilibrium equation system is as follows:

$$k\delta = F \quad (14)$$

(4) Solving the System of Global Equilibrium Equations

3. ENGINEERING EXAMPLES

3.1 Project Overview

The Chushandian Dam is in the construction period, so it only needs to consider that the upstream is at the normal height water level. The foundation of the dam is equipped with an anti-seepage curtain, which can not consider the downstream water seepage. The force on the dam body is shown in Fig. 4. The elevation of normal height water level is 88m. The research object of this study is the barrage section of the Chushandian gravity dam, which is a type of gravity dam. The elevation of the dam foundation is 65m. The research dam section is from 12 # to 15 #. The crest elevation of dam sections 12 # and 13 # is 83 m. The floor elevation of the bottom outlet inlet gate of dam sections 14 # and 15 # is 75 m. The crest elevation of dam section 12 # ~15 # is 100.3 m. The total length of dam sections 12 # ~15 # is 79.95 m (including joint width). The main material models of the dam body include C20, C25 concrete, etc.
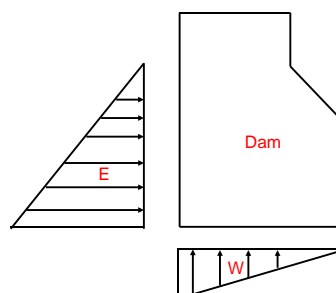
Fig. 4. Dam body force diagram

3.2 Model Parameters and Model Establishment

Taking the typical overflow dam section 12 # ~15 # of Chushandian Reservoir as the research object, the dam section has a height of 35.3m and a length of 79.95m. To minimize the impact of boundary conditions on the simulation results of the dam body, a sufficiently large foundation should be selected for finite element analysis. The simulation range of the foundation is shown in Fig. 5, which extends horizontally from the dam heel and toe to the upstream and downstream by 2.5 times the dam height. Extend the dam height by two times vertically from the dam foundation surface downwards. The Dam axis is extended 2.5 times the dam height. The finite element model element is C3D8R, with a total of 1877 nodes and 3699 elements. The dam body is made of C20 concrete, and the standard compressive strength of C20 concrete is 20 MPa, and the standard tensile strength is 1.54 MPa. The elastic moduli of the dam body and foundation are 24 GPa and 22.5GPa, with densities of 2400 kg/m^3 and 2600 kg/m^3, and Poisson's ratios of 0.167 and 0.25, respectively.

3.3 Boundary Condition

(1) The foundation part of the dam model is completely fixed. (2) Due to the construction

73

period of the dam, there is no hydrostatic pressure downstream of the dam. (3) The upstream of the dam body is subjected to hydrostatic pressure, while the downstream dam foundation is considered to have uplift pressure. (4) The working condition of normal height water level (the elevation of normal height water level is 88m, and the elevation of dam foundation is 65m) is selected as the calculation condition. (5)The dam body is co-noded with the foundation.
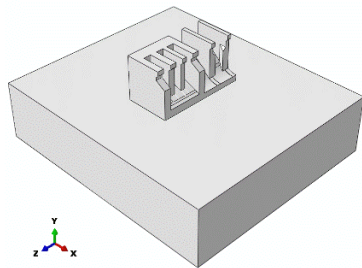

Fig. 5. Finite element model diagram

3.4 Analysis of Numerical Simulation Results

3.4.1 Stress analysis

The first principal stress cloud diagram of the dam is shown in Fig. 6. From Fig. 6, it can be seen that the maximum stress is located in the overflow dam section. In the overflow dam section, the stress concentration part is located at the junction of the transverse joint and the upper curve section of the overflow dam surface. In addition, there is also a phenomenon of stress concentration at the heel of the dam, but there is no obvious overflow in the dam section. There is no tensile stress zone at the dam heel, which meets the stress requirements. Overall, the overall stress of the dam is relatively small, mostly not exceeding 1MPa. Only in the overflow dam section and the dam heel area did significant stress occur, but the maximum value

at both locations was 19MPa. 19MPa is less than the compressive strength of the material. There is a small compressive stress at the toe of the dam, with a value of 1.1 MPa, which is much smaller than the compressive strength of the material. The maximum principal stress is located at the joint between the transverse joint of the overflow dam section and the upper curve, which is a dangerous area. The minimum value is located at the crest of the dam section. It can be seen from the stress diagram as a whole that the stress of the dam body is small under the condition of normal height water level, which meets the strength requirements of materials. The dam is in a safe state as a whole.

3.4.2 Displacement analysis

The displacement cloud map of the dam is shown in Fig. 7. From Fig. 7, it can be seen that the overall displacement of the dam is in the range of 10^{-2}. The maximum displacement position is located in the overflow dam section. The displacement of the overflow dam section decreases sequentially from the top to the bottom. The value at the dam crest is 35mm. The displacement of the surface hole dam section also decreases from top to bottom, with a maximum displacement of 23mm. The displacement of the dam foundation is the smallest and close to zero. The direction of displacement under static load is all rightward displacement. The displacement of the dam from the top to the bottom exhibits a clear zoning phenomenon. The crest of the overflow dam section is the most easily damaged part of the dam body, but considering its maximum displacement value of 35 mm, it meets the displacement requirements. Therefore, it is only necessary to monitor and reinforce the dam crest area. From the overall displacement distribution diagram of the dam, it can be seen that the dam is in a safe state.
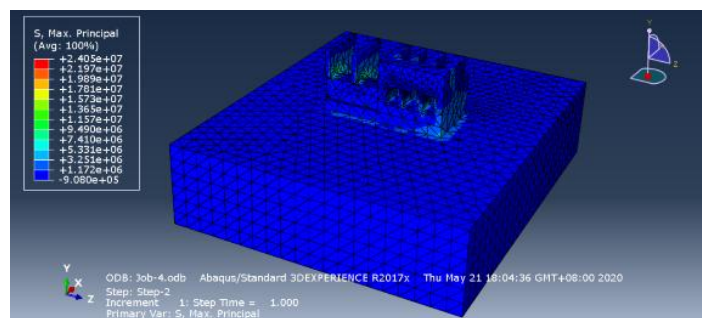

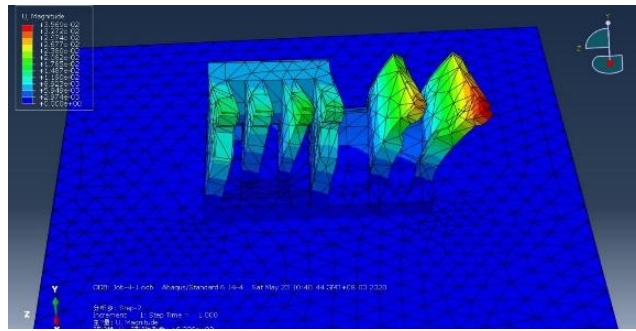**Fig. 6. Cloud chart of the first principal stress of the dam**

Fig. 7. Cloud map of dam displacement

3.4.3 Modal result analysis

In the visualization module, the first ten modal diagrams of the model are shown in Figs. 8 to 17, Table 1.
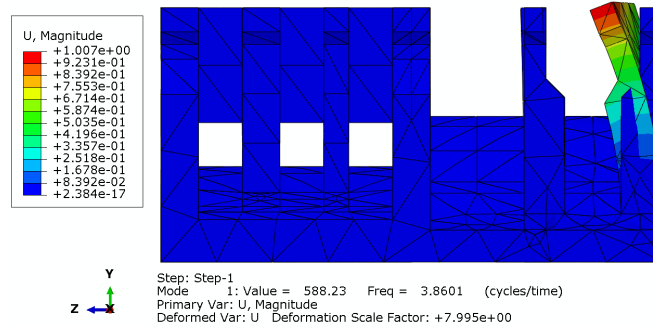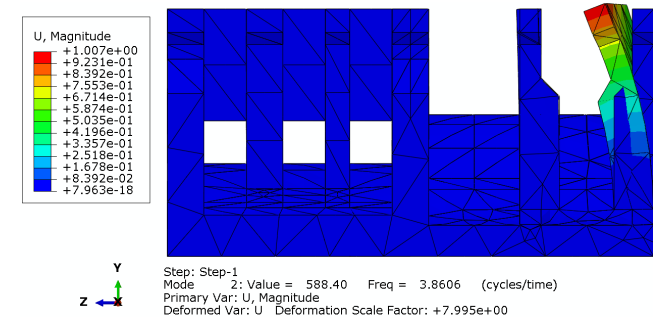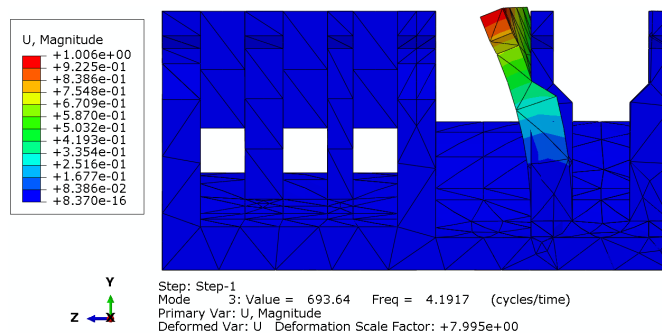

Fig. 8. First order
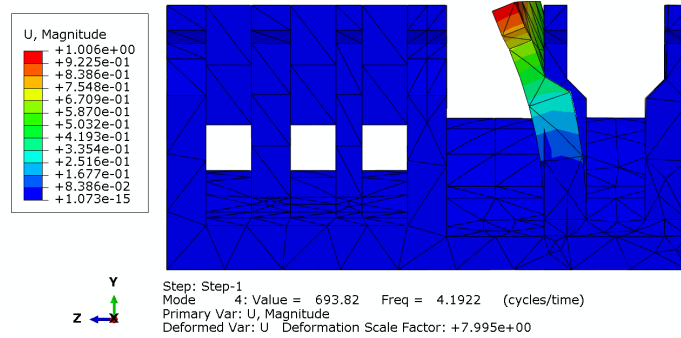

Fig. 9. Second order
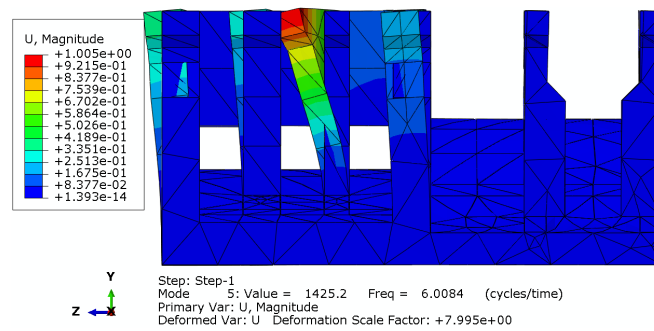

Fig. 10. Third order
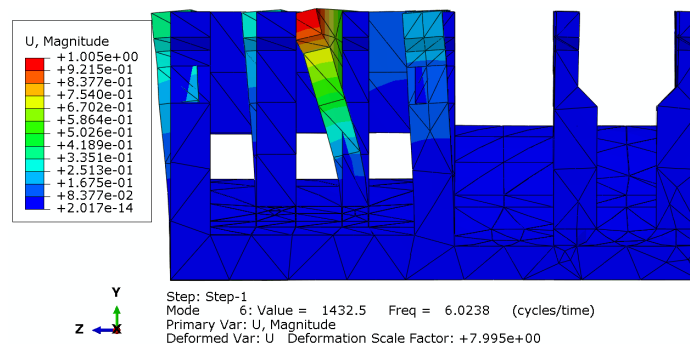
Fig. 11. Fourth order
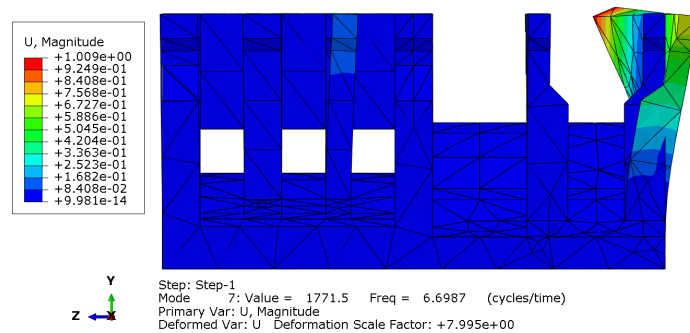

Fig. 12. Fifth order

Fig. 13. Sixth order
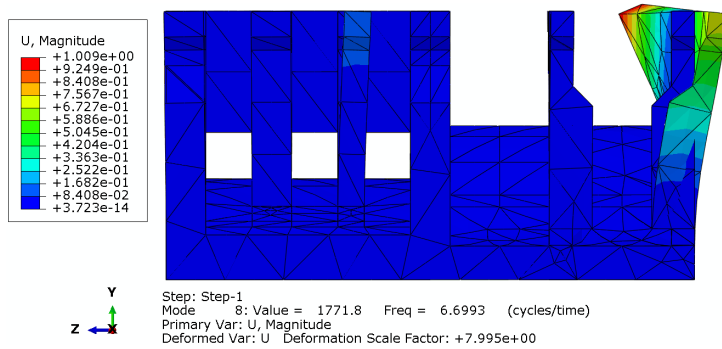

Fig. 14. Seventh order
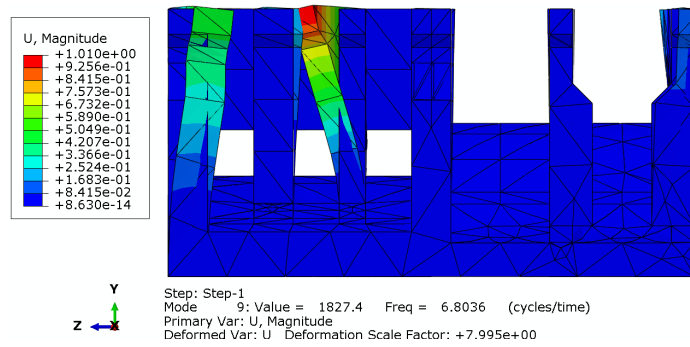
Fig. 15. Eighth order

Fig. 16. Ninth order
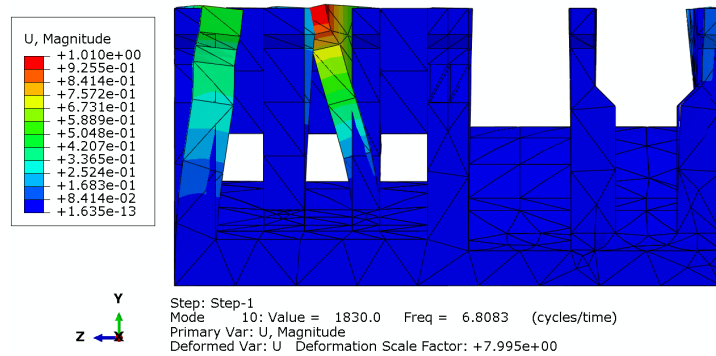
Fig. 17. Tenth order

Table 1. Table of the first ten orders

No frequency	frequency, Hz	Contribution coefficient		
		Axis X	Axis Y	Axis Z
1	3.8601	0.2344	0.0155	1
2	3.8606	1	0.0505	0.2544
3	4.1917	0.0005	0.0006	1
4	4.1922	0.0751	1	0.0005
5	6.0084	0.0003	0.0018	0.3997
6	6.0238	0.2379	0.1198	0.0001
7	6.6987	0	0.0003	0.0021
8	6.6993	0.0076	0.0077	0.0003
9	6.8036	0.0005	0.0003	0.0068
10	6.8083	0.0046	0.0025	0.0007

From Figs. 8 to 17 and Table 1, it can be seen that the color changes in the first order vibration mode diagram indicate that at the lowest vibration frequency, that is, at the first order, the most obvious deformation is at the right most part of the dam crest. When the vibration frequency is low, the top part of the dam on the right side of the dam responds more significantly to the first order vibration frequency, and the deformation of the top part on the right side of the dam is more severe; In the second-order vibration mode diagram, the area with significant deformation of the dam is still on the right side of the dam top, indicating that the area on the right side of the dam top still has a significant response to the second-order vibration frequency, but the deformation is more severe than in the first-order vibration mode diagram; In the third order vibration mode diagram, the dam with large deformation is still at the dam crest, but the position with obvious response moves to the left of the dam Dam axis; In the fourth order vibration mode diagram, the deformation part of the dam is the same as the third order, but the degree of deformation has increased; In the seventh order vibration mode diagram, at the seventh order vibration frequency, the most obvious response part is still at the top of the dam, but it has twisted from the previous backwater side to the upstream side. The most obvious response part in the subsequent eighth, ninth, and tenth order vibration mode diagrams is still on the upstream side of the dam top. After observing the first to tenth order vibration mode diagrams, the following pattern was found: in the gravity dam model, the large deformation parts of the dam mainly occur at the top of the dam; As the vibration frequency increases, the deformation becomes more and more severe; With the increase of frequency, the easily deformed parts are constantly changing along the Dam axis. Specifically, in the first to sixth order mode shapes, with the increase of vibration frequency, the deformed parts gradually move from the dam crest on the right side of the model to the left side of the dam crest, and the displacement of the deformed parts is constantly increased to the left. In the sixth to seventh order mode shapes, the easily deformed parts move from the left side of the dam to the right side of the dam, And the direction of the deformation part has changed from displacement to displacement to the right. In the seventh to tenth order vibration mode diagrams, the moving part has moved again from the right side of the dam to the left side of the dam, and the direction of

the deformation part continues to increase the displacement to the right.

In summary, under external excitation, cracks are most likely to occur at the top of the dam, which is prone to significant response phenomena at lower frequencies. Therefore, it is necessary to pay special attention to the cracking situation at the top of the dam and the reinforcement of the top of the dam; Although the natural vibration phenomenon of the dam is not easy to detect, it is real; Under the excitation of certain external frequencies, the phenomenon of response at the top of the dam is significantly higher than that at the bottom of the dam; The response position at the top of the dam will constantly change back and forth on the upstream and downstream sides with the continuous change of frequency. At this time, the displacement direction at the deformation point is also constantly changing, and the degree of deformation gradually increases with the increase of frequency.

4. CONCLUSION

The conclusions are as follows:

(1) Under the condition of normal height water level, there is a small tensile stress at the dam heel, and the compressive stress at the dam toe is within the normal range. There is significant stress at the intersection of the upper curved part of the overflow dam and the transverse joint. The dam body strength meets the requirements and can be considered safe for the reservoir.

(2) Modal analysis of the model reveals that significant deformation can occur at the right side of the dam crest during lower frequency vibrations. With the increasing frequency, the easily deformed parts of the dam are still at the top of the dam, and the displacement of the easily deformed parts is increasing, and the position of the easily deformed parts is moving along the Dam axis, and the deformation direction of the easily deformed parts will change regularly.

COMPETING INTERESTS

Author has declared that no competing interests exist.

REFERENCES

1. Fu Zhongyou, Zhang Shichen. Analysis of failure modes and paths of gravity dams based on engineering examples [J]. Water

Conservancy and Hydropower Technology. 2010,41(09):57-60+71.

2. Yang Feng, Ni Yufang, Huang Wei，et al. Numerical Simulation of Dam Break Flood in Chushandian Reservoir [J]. Yellow River. 2020,42(01):27-31+36.

3. Zhang Xiuli. Collection of Typical Cases of Dam Accidents or Hydropower Station Accidents at Home and Abroad [J]. Dams and Safety. 2015;87(01): 13-16.

4. Feng Ping. Analysis of Concrete Gravity Dams Based on ANSYS Software [J]. Technological Innovation and Application. 2018(29):55-56.

5. Xue Song. Finite Element Static and Dynamic Analysis of High Concrete Gravity Dams Based on ANSYS [D]. North China University of Water Resources and Hydropower; 2018.

6. Wang Yi. Three dimensional finite element numerical simulation analysis of anti sliding stability of gravity dams [J]. Water Conservancy Planning and Design. 2019 (09):62-63+139.

7. Cheng Lu, Ye Yong. Finite Element Analysis of Design Water Level for High Chair Gravity Dam [J]. Water Conservancy Technology and Economy. 2019,25(07):12-14+38.

8. Xu Nana. 3D Finite Element Analysis and Section Optimization Design of Gravity Dams [D]. Lanzhou University of Technology; 2019.

9. Guo Bingqiao, Mo Jiyun. Numerical simulation of multiple cracks in concrete gravity dams based on extended finite element method [J]. Science and Technology and Engineering; 2019;19(15): 298-302.

10. Jin Yusong. Finite element analysis of bonding between concrete gravity dams and high-tech old concrete [D]. Zhengzhou University; 2019.

11. Zhang Long, Yang Peng, Zhang Lexuan. Three dimensional finite element analysis of the masonry gravity dam of Nanhu Reservoir in Huixian County, Henan Province [J]. Journal of Yellow River Water Conservancy Vocational and Technical College. 2017;29(04):4-8.

12. Zhou Dynasty, Zhang Ziqin. Three dimensional finite element analysis of concrete gravity dams [J]. Technological Innovation and Application. 2016(36): 23-24.

Peer-review history:
The peer review history for this paper can be accessed here:
https://www.sdiarticle5.com/review-history/99530